

1   **Equilibrium climate sensitivity increases with aerosol concentration**  
2   **due to changes in precipitation efficiency**

3   Guy Dagan<sup>1\*</sup>

4   <sup>1</sup> Fredy and Nadine Herrmann Institute of Earth Sciences, Hebrew University,  
5   Jerusalem, Israel

6   \*Corresponding author. Email: [guy.dagan@mail.huji.ac.il](mailto:guy.dagan@mail.huji.ac.il)

7

8

9

10

11

12

13

14

15

16

17

18

19

20

21

22

23

24

25

26

27

28

29

30

31

32

33

35      **Abstract**

36      How Earth's climate reacts to anthropogenic forcing is one of the most burning  
37      questions faced by today's scientific community. A leading source of uncertainty in  
38      estimating this sensitivity is related to the response of clouds. Under the canonical  
39      climate-change perspective of forcings and feedbacks, the effect of anthropogenic  
40      aerosols on clouds is categorized under the forcing component, while the modifications  
41      of the radiative properties of clouds due to climate change are considered in the  
42      feedback component. Each of these components contributes the largest portion of  
43      uncertainty to its relevant category and is largely studied separately from the other. In  
44      this paper, using idealized cloud resolving, radiative-convective-equilibrium  
45      simulations, with a slab ocean model, we show that aerosol-cloud interactions could  
46      affect cloud feedback. Specifically, we show that equilibrium climate sensitivity  
47      increases under high aerosol concentration due to an increase in the shortwave cloud  
48      feedback. The shortwave cloud feedback is enhanced under high aerosol conditions due  
49      to a stronger increase in the precipitation efficiency with warming, which can be  
50      explained by higher sensitivity of the droplet size and the cloud water content to the  
51      CO<sub>2</sub> concentration rise. These results indicate a possible connection between cloud  
52      feedback and aerosol-cloud interactions.

53

54      **1. Introduction**

55      Estimating Earth's equilibrium climate sensitivity (ECS), defined as the steady-state  
56      global mean temperature increase for a doubling of CO<sub>2</sub>, is considered as a first-order,  
57      fundamental milestone on the way to understanding and predicting anthropogenic-  
58      driven climate change (Sherwood et al., 2020). Decades of research have tried to  
59      accurately quantify ECS, with only limited success. The most probable current ECS  
60      estimates are in the range of 2.3–4.5K (Sherwood et al., 2020). The largest source of  
61      uncertainty in estimating ECS is related to the response of clouds to the externally  
62      forced warming and the feedback of these changes on the climate system (Sherwood et  
63      al., 2020; Ceppi et al., 2017; Schneider et al., 2017). Clouds strongly modulate Earth's  
64      radiation budget by reflecting the incoming shortwave radiation from the sun and by  
65      absorbing and re-emitting the terrestrial longwave radiation (Loeb et al., 2018). Thus,  
66      changes in the cloud macro-physical properties (such as coverage and vertical extent)  
67      and micro-physical properties (such as liquid/ice partition or hydrometeors size) due to  
68      anthropogenic-driven climate change could significantly alter the climate system's

pmw: significantly

pmw: strong

71 response (Gettelman and Sherwood, 2016; Nuijens and Siebesma, 2019; Schneider et  
72 al., 2017).

73 An important factor in determining cloud feedback magnitude is the sensitivity of the  
74 Precipitation Efficiency ( $\epsilon$ ) (Lutsko et al., 2021; Li et al., 2022; Lutsko and Cronin,  
75 2018).  $\epsilon$  quantifies the fraction of condensed water in a cloud to reach the surface as  
76 precipitation. Using idealized cloud resolving simulations, it was shown that  $\epsilon$  is  
77 expected to increase with temperature (Lutsko and Cronin, 2018). The increase in  $\epsilon$   
78 with warming was shown to be mostly driven by an increase in the efficiency with  
79 which cloud condensate is converted into precipitation, while changes in the  
80 evaporation of falling precipitation was shown to play a smaller role (Lutsko and  
81 Cronin, 2018).

82 more efficiently depletes An increase in  $\epsilon$  with warming represents more efficient depletion of the water from  
83 the clouds, thus affecting the radiation budget. On the one hand, increase in  $\epsilon$  with  
84 warming was suggested to reduce the anvil cloud coverage and hence increase the  
85 outgoing longwave radiation (Lindzen et al., 2001; Mauritsen and Stevens, 2015), thus  
86 producing negative feedback. On the other hand, however, it was recently shown that  
87 the longwave effect of an  $\epsilon$  increase is over-compensated for by changes in the  
88 shortwave flux (Li et al., 2019), i.e., a large reduction in the cloud optical depth, driving  
89 a reduction in the shortwave cooling effect of clouds, dominates the response.

90 The efficiency with which cloud condensate is converted into precipitation is closely  
91 linked to the micro-physical properties of the clouds. The autoconversion of cloud  
92 droplets into rain becomes significant when liquid water amount and/or droplet radii  
93 reach a critical threshold (Freud and Rosenfeld, 2012). An important factor influencing  
94 the droplet radii (and also the liquid water amount, to some degree) is the amount of  
95 available cloud condensation nuclei (CCN). Generally, an increase in aerosol  
96 concentration drives an increase in CCN concentration, which results in more numerous  
97 and smaller droplets in the cloud (Twomey, 1974; Warner and Twomey, 1967). The  
98 smaller droplets require longer time (or equivalently larger vertical distance) in the  
99 clouds to grow by diffusion to the critical size enabling precipitation, thus delaying the  
100 initial warm rain formation (Rosenfeld, 2000; Dagan et al., 2015b). In addition, aerosols  
101 were suggested to enhance the vertical velocities and the cloud top heights of deep  
102 convective clouds (due to the so-called invigoration mechanism (Abbott & Cronin,  
103 2021; Koren et al., 2005; Rosenfeld et al., 2008)), which in turn can results in

105 [precipitation enhancement](#) (Koren et al., 2012). Therefore, aerosols could affect  $\epsilon$   
106 (Khain, 2009).

107 In addition to the effect on rain, aerosols could modify the radiative properties of clouds,  
108 by modifying the droplet concentration and size distribution (Twomey, 1974) and by  
109 affecting the clouds' macro-physical properties (Albrecht, 1989; Bellouin et al., 2019).  
110 These changes to the radiative properties of clouds result in radiative forcing that could  
111 affect the sea surface temperature [SST (Bellouin et al., 2019)]. Using cloud-resolving  
112 radiative-convective-equilibrium simulations with interactive SST, Khairoutdinov and  
113 Yang (2013) showed that the surface temperature decreases by 1.5K with each 10-fold  
114 increase in aerosol concentration, an effect quite comparable to a 2.1–2.3K SST  
115 warming obtained in a simulation with given (low) aerosol conditions but doubled CO<sub>2</sub>  
116 concentration.

117 It has been suggested that cloud feedback and aerosol forcing are not independent of  
118 each other (Mülmenstädt and Feingold, 2018; Igel and van den Heever, 2021). In  
119 addition, the strong links between  $\epsilon$  and cloud feedback and between  $\epsilon$  and aerosol  
120 concentration merit a dedicated study on the potential mutual CO<sub>2</sub> and aerosol effect on  
121 clouds and thus also on ECS, which is the aim of the current study.

122

123

124 **2. Methods**

125 **Model description and experimental design**

126 The model used herein is the System of Atmospheric Modeling [SAM - (Khairoutdinov  
127 and Randall, 2003)] version 6.11.7. Subgrid-scale fluxes are parameterized using  
128 Smagorinsky's eddy diffusivity model and gravity waves are damped at the top of the  
129 domain. The microphysics scheme used is Morrison et al. (2005) 2-moment bulk  
130 microphysics. The cloud droplet number concentration source assumes that the number  
131 of activated CCN depends on the super-saturation ([S – which is estimated diagnostically  
132 in the model as the model assumes saturation adjustment](#)) according to a power-law:  
133  $CDNC = N_a S^k$ , where  $N_a$  is the prescribed concentration of CCN active at 1 % super-  
134 saturation, and  $k$  is a constant (set in this study to 0.4 - a typical value for maritime  
135 conditions). Changes in  $N_a$  serve as a proxy for the change in aerosol concentration.  
136 Three levels of  $N_a$  are considered here, covering an extreme range of conditions – 20,  
137 200 and 2000 cm<sup>-3</sup>. While this wide range of conditions is unlikely to exist at any given

pmw: computes

pmw: ius for

138 geographical location, they are used here in order to cover the range of possible  
139 conditions at different locations and to maximize the effect for establishing better  
140 physical understanding. The activation of CCN at the cloud base is parameterized  
141 following Twomey (1959), using the vertical velocity and CCN spectrum parameters.

142 The model is configured to pass cloud water and ice-crystal effective radii, from the  
143 microphysics scheme to the radiation scheme; thus, the Twomey effect (Twomey,  
144 1977) of both liquid and ice is considered. Direct interactions between aerosols and  
145 radiation are not considered here.

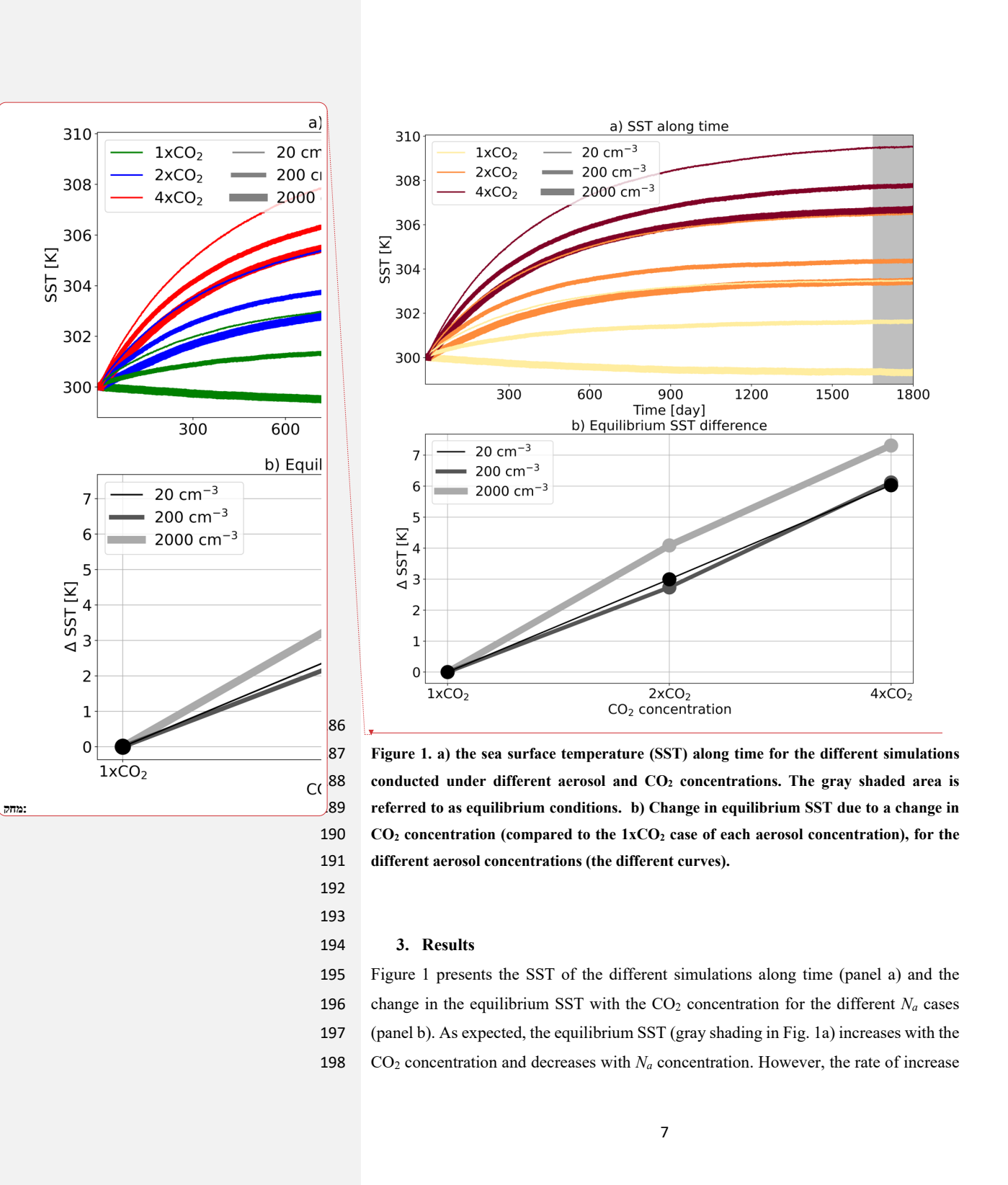
146 The simulations are conducted in a radiative-convective-equilibrium (RCE) mode and  
147 generally follow the RCEMIP (RCE model inter-comparison project (Wing et al.,  
148 2018)) small-domain instructions (but with interactive SST and changes in the CO<sub>2</sub> and  
149 aerosol concentration). The simulations were performed on a square, doubly periodic  
150 domain. In this case, we want to avoid the effect of convective self-aggregation on  $\epsilon$ ;  
151 thus, the domain size is set to 96x96 km<sup>2</sup>, which was shown to be small enough to  
152 prevent convective self-aggregation (Muller and Held, 2012; Lutsko and Cronin, 2018;  
153 Yanase et al., 2020). The horizontal grid spacing is set to 1km and 68 vertical levels are  
154 used, between 25m and 31km, with vertical grid spacing increasing from 50m near the  
155 surface to roughly 1km at the domain top. We note that while shallow clouds are present  
156 in the simulations, the grid spacing used here is too coarse for a full representation of  
157 these clouds. A time step of 10s is used, and radiative fluxes are calculated every 5 min  
158 using the CAM radiation scheme (Collins et al., 2006). The output resolution for all  
159 fields is 1h. (3D fields are saved as snapshots while domain statistics are saved as  
160 hourly-averages). The incoming solar radiation is fixed at 551.58 Wm<sup>-2</sup> with a zenith  
161 angle of 42.05° (Wing et al., 2018), producing a net insolation close to the tropical-  
162 mean value. Convection is initialized with a small thermal noise added near the surface  
163 at the beginning of the simulation. The initial conditions for the simulations are as in  
164 Wing et al. (2018).

165 Greenhouse gases are varied for three different levels: pre-industrial level (280 PPM,  
166 1xCO<sub>2</sub>), 2 times pre-industrial level (2xCO<sub>2</sub>) and 4 times pre-industrial level (4xCO<sub>2</sub>).  
167 As in the case of the aerosol concentrations, the large range of CO<sub>2</sub> conditions covered  
168 here are used to examine the clouds' sensitivity to greenhouse gas concentrations under  
169 a wide range of conditions. Nine different simulations, with all possible combinations  
170 of  $N_a$  and CO<sub>2</sub> concentrations, were conducted. The O<sub>3</sub> vertical profile is similar to

173 [Wing et al. \(2018\) and represents a typical tropical atmosphere. The effect of other trace](#)  
174 [gases \(such as CH<sub>4</sub> and N<sub>2</sub>O\) is neglected for simplicity.](#)

175 In all simulations, the SST is interactive and predicted by a slab ocean model (SOM).  
176 The SOM's mixed layer depth is set to 5m, which represented a compromise between a  
177 relatively deep layer ( $\geq 10$ m), which reduces SST noise (Khairotdinov and Yang,  
178 2013), and a relatively shallow layer ( $\ll 1$ m), which requires a shorter computation time  
179 for equilibrium (Romps, 2020). As in Romps (2020), the SOM is cooled at a rate of 112  
180  $\text{Wm}^{-2}$  in order to ensure that the simulations with 1xCO<sub>2</sub> are kept at around the initial  
181 SST of 300K (Fig. 1). Each simulation was run for 1800 days, which is sufficient for  
182 reaching close to equilibrium (the surface energy imbalance is  $\leq 0.1 \text{Wm}^{-2}$  in all  
183 simulations during the last 150 days). The last 150 days of each run are used for  
184 statistical sampling (gray shading in Fig. 1).

185



200 in equilibrium SST with CO<sub>2</sub> concentration increases under extremely high  $N_a$   
201 concentrations (2000 cm<sup>-3</sup>), compared with the low and medium  $N_a$  concentrations (20  
202 and 200 cm<sup>-3</sup>, respectively - Fig. 1b). Calculating the average ECS based on the three  
203 combinations available for each  $N_a$  condition [2xCO<sub>2</sub>-1xCO<sub>2</sub>, 4xCO<sub>2</sub>-2xCO<sub>2</sub> and  
204 (4xCO<sub>2</sub>-1xCO<sub>2</sub>)/2], demonstrates that it increases with  $N_a$  from 3.0K at the lowest  $N_a$   
205 to 3.7K at the highest  $N_a$  (i.e., a 23% increase – Table 1).

206

207 **Table 1. Average equilibrium climate sensitivity (ECS), cloud-feedback parameter ( $\lambda_{\text{cloud}}$ ),**  
208 **hydrological sensitivity ( $\eta$ ), and change in precipitation efficiency ( $\Delta\epsilon$ ) of the three**  
209 **combinations available for each  $N_a$  condition [2xCO<sub>2</sub>-1xCO<sub>2</sub>, 4xCO<sub>2</sub>-2xCO<sub>2</sub> and 4xCO<sub>2</sub>-**  
210 **1xCO<sub>2</sub>]. For the calculation of the average ECS, the difference between 4xCO<sub>2</sub> and 1xCO<sub>2</sub>**  
211 **is divided by 2. The rest of the quantities are normalized by the SST change between the**  
212 **relevant simulations. Please refer to the text for the definitions of these quantities.**

$N_a$ [cm <sup>-3</sup> ]	ECS [K]	$\lambda_{\text{cloud}}$ [W m <sup>-2</sup> K <sup>-1</sup> ]	$\eta$ [% K <sup>-1</sup> ]	$\Delta\epsilon$ [% K <sup>-1</sup> ]
20	3.0	-0.45	3.8	1.2
200	3.1	-0.38	4.3	1.3
2000	3.7	-0.08	4.6	2.7

213

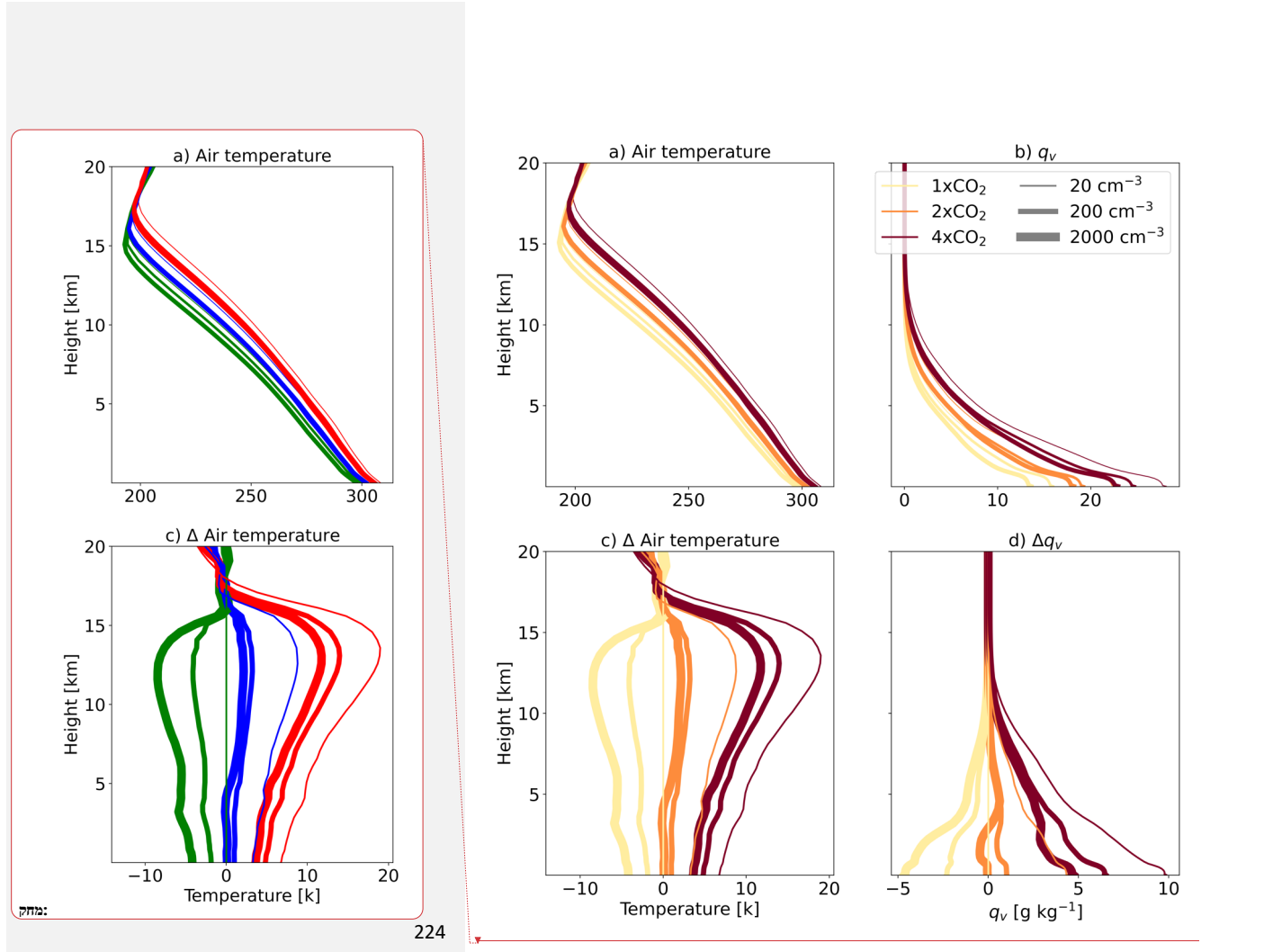
214 Figure 2 presents the time and domain mean vertical profiles of temperature and water  
215 vapor mixing ratio ( $q_v$ ) in the different simulations (panels a and b) and their difference  
216 from the simulation with the lowest  $N_a$  and CO<sub>2</sub> concentrations (panels c and d). It  
217 demonstrates, as expected, that the vertical profile of air temperature is set by the  
218 surface temperature (increases with CO<sub>2</sub> concentrations and decreases with  $N_a$ ) with an  
219 amplification of the change at the upper troposphere, as the profiles follow the moist  
adiabatic lapse-rate. It also shows that  $q_v$  increases with the temperature, as expected  
(Held and Soden, 2006).

220

221

222

pmw:  $q_v$



224  
225 **Figure 2. Time and domain mean vertical profiles of air temperature and water vapor  
226 mixing ratio ( $q_v$ ) in the different simulations (a and b) and how they differ from the  
227 simulation with the lowest  $N_a$  and CO<sub>2</sub> concentrations (panels c and d).**  
228  
229

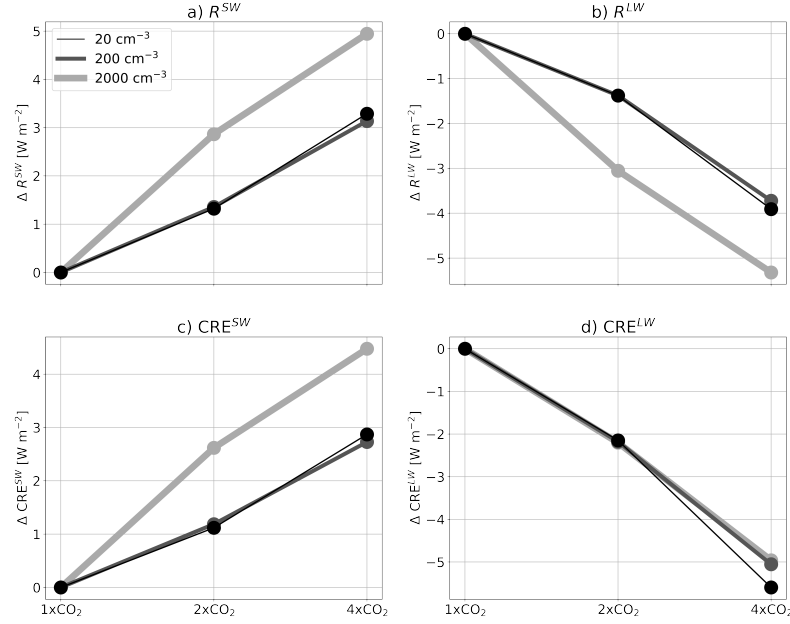
230 In order to understand the increase in ECS with  $N_a$ , we next examine the top-of-  
231 atmosphere (TOA) energy budget. Figure 3 presents the change in the net shortwave  
232 and longwave TOA energy gain ( $R^{SW}$  and  $R^{LW}$ , respectively) with the CO<sub>2</sub>  
233 concentration for the different  $N_a$  conditions. In addition, Fig. 3 presents the change in  
234 the cloud radiative effect (CRE) with increasing the CO<sub>2</sub> concentration, where CRE is  
235 computed by subtracting the clear-sky from the all-sky TOA radiative fluxes

37 עיבוד: לא נתוי, גופן עברית ושותות אחרות: לא  
38 כתוי

( $R - R_{\text{clear-sky}}$ ), again for the shortwave and longwave separately ( $\text{CRE}^{\text{SW}}$  and  $\text{CRE}^{\text{LW}}$ , respectively). Figure 3a and b demonstrates that under equilibrium conditions  $R^{\text{SW}}$  increases, while  $R^{\text{LW}}$  decreases with the  $\text{CO}_2$  concentration. However, the rate of change in both  $R^{\text{SW}}$  and  $R^{\text{LW}}$  is much faster under the high  $N_a$  conditions than under the low and medium  $N_a$  conditions. The trend in  $\text{CRE}^{\text{SW}}$  under the different  $N_a$  conditions (Fig. 3c) resembles the trend in  $R^{\text{SW}}$ , suggesting that the clouds' response dominates the changes in the TOA shortwave fluxes.  $\text{CRE}^{\text{LW}}$ , on the other hand, decreases at a similar rate with  $\text{CO}_2$  concentration for the different  $N_a$  conditions (Fig. 3d). Thus, the different decrease rates in  $R^{\text{LW}}$  with  $\text{CO}_2$  concentration for the different  $N_a$  conditions (Fig. 3b) must be driven by clear-sky changes (specifically, the plank, the lapse-rate and the water vapor feedbacks – see Fig. 2 above).

239  
240  
241  
242  
243  
244  
245  
246  
247  
248  
249  
250  
251  
252  
253  
254  
255

In Table 1 above, we estimate the average cloud radiative feedback ( $\lambda_{\text{cloud}}$ ) as the change in CRE with increasing surface temperature, i.e.,  $\lambda_{\text{cloud}} = d\text{CRE}/dT$ , for the different  $N_a$  conditions. The table shows that  $\lambda_{\text{cloud}}$  becomes less negative with the increase in  $N_a$ , leading to higher climate sensitivity. The differences in the values of  $\lambda_{\text{cloud}}$  between the different  $N_a$  conditions is mostly derived from the shortwave part of the spectrum (Fig. 3).



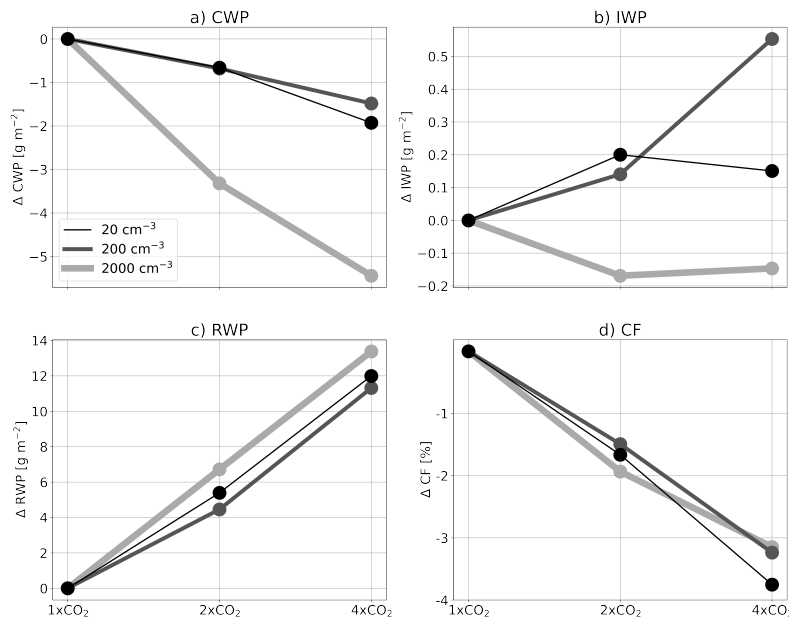
257  
258 **Figure 3. The change in the net top-of-atmosphere energy gain ( $R$ ) in the shortwave (a)**  
259 **and in the longwave (b), and the change in the cloud radiative effect (CRE) in the**  
260 **shortwave (c) and in the longwave (d), due to a change in the CO<sub>2</sub> concentration**  
261 **(compared to the 1xCO<sub>2</sub> case of each aerosol concentration), for the different aerosol**  
262 **concentrations (the different curves).**

263  
264 Thus far, we have seen that the ECS increases with  $N_a$  (Fig. 1 and Table 1) and that this  
265 increase can be explained by changes in  $\lambda_{cloud}$  (Table 1) and specifically in  $CRE^{SW}$  (Fig.  
266 3). To understand the changes in the cloud properties driving the changes in  $\lambda_{cloud}$ , and  
267 hence also in ECS, under the different  $N_a$  conditions, in Fig. 4 we present the change in  
268 cloud liquid water path (CWP), ice water path (IWP), rain water path (RWP) and cloud  
269 fraction (CF) with increasing CO<sub>2</sub> concentrations for the different  $N_a$  conditions. The  
270 figure shows that the CWP decreases with the CO<sub>2</sub> concentrations at a much faster rate  
271 (about 3 times faster) under the highest  $N_a$  conditions compared to the low and medium  
272  $N_a$  conditions (Fig. 4a). The changes in the IWP, on the other hand, are about an order  
273 of magnitude smaller than the changes in CWP and are not consistent in sign for the  
274 different  $N_a$  conditions (Fig. 4b). The RWP increases with the CO<sub>2</sub> concentrations at a  
275 slightly faster rate (about 20% faster) under the highest  $N_a$  conditions compared to the

276 low and medium  $N_a$  conditions (however the response is non-monotonic with  $N_a$  - Fig.  
 277 4c). The CF decreases with the  $\text{CO}_2$  concentrations, at a similar rate for the different  $N_a$   
 278 conditions (about 1.5% decrease in CF for each doubling of the  $\text{CO}_2$  concentrations -  
 279 Fig. 4d).

280 The faster decrease in CWP with  $\text{CO}_2$  concentrations under high  $N_a$  conditions drives  
 281 the faster increase in  $\text{CRE}^{\text{SW}}$  as the clouds become less opaque in the shortwave. We  
 282 note that the difference in  $\text{CRE}^{\text{SW}}$  trend under different  $N_a$  conditions could not be  
 283 explained by the minor differences in the CF trends. In addition, the small differences  
 284 in the IWP between the different  $N_a$  conditions are consistent with the small differences  
 285 in the  $\text{CRE}^{\text{LW}}$  seen above. The general increase in RWP with  $\text{CO}_2$  concentrations is  
 286 consistent with an increase in rain efficiency with warming (Lutsko and Cronin, 2018),  
 287 as elaborated below.

288  
 289



290  
 291 **Figure 4. The change in: a) cloud liquid water path (CWP), b) ice water path (IWP, c)  
 292 rain water path (RWP), and d) cloud fraction (CF) due to a change in the  $\text{CO}_2$   
 293 concentration (compared to the  $1x\text{CO}_2$  case of each aerosol concentration), for the  
 294 different aerosol concentrations (the different curves).**

295 Figure 4 suggests that the largest difference in the cloud response to CO<sub>2</sub> under different  
296  $N_a$  conditions is due to changes in CWP. The higher sensitivity of CWP to CO<sub>2</sub>  
297 concentration under higher  $N_a$  conditions can explain the higher  $\lambda_{\text{cloud}}$  and thus also the  
298 larger ECS. Hence, the question arises: What causes the faster reduction in CWP with  
299 CO<sub>2</sub> concentration under high  $N_a$  conditions? A major sink for CWP is via precipitation.  
300 Hence, in Fig. 5 we present the change in the mean surface precipitation rate, the  
301 hydrological sensitivity ( $\eta$  - the rate of change in the surface precipitation per 1K  
302 increase in surface temperature) and the precipitation efficiency ( $\epsilon$ - calculated  
303 following Li et al. (2022) as the ratio of surface precipitation-to-condensed water path,  
304 i.e., CWP+IWP+RWP). [Please note that the precipitation efficiency definition used  
here, following Li et al. \(2022\), is slightly different from the definition used in Lutsko  
and Cronin \(2018\). However, the two different definitions were shown to be tightly  
correlated \(Li et al., 2022\), thus, the exact definition used is not expected to change the  
main conclusions. In addition, the use of this definition will enable easier comparison  
with observations and global climate models in the future.](#)

310 As expected, [Fig. 5 demonstrates that](#) the surface precipitation increases with CO<sub>2</sub> (i.e.,  
311  $\eta$  is positive) and so does  $\epsilon$  (Lutsko and Cronin, 2018). This is true for all  $N_a$  conditions.  
312 However, the rates of increase in surface precipitation and  $\epsilon$  with CO<sub>2</sub> concentration  
313 are higher under the highest  $N_a$  conditions (see also Table 1). We note that the larger  
314 rate of increase in surface precipitation under the highest  $N_a$  conditions is not solely due  
315 to the higher surface temperature increase, as  $\eta$  also increases with  $N_a$ .

316 The much larger (more than double- Table 1) rate of increase in  $\epsilon$  with the CO<sub>2</sub>  
317 concentration under the highest  $N_a$  conditions [represents more efficient depletion of](#) the  
318 cloud water [from the atmosphere](#), leading to a faster reduction in CWP with CO<sub>2</sub>  
319 concentration (Fig. 4), which in turn leads to higher  $\lambda_{\text{cloud}}$  and ECS. The faster increase  
320 in RWP with CO<sub>2</sub> concentration under the highest  $N_a$  conditions presented in Fig. 4c is  
321 consistent with this explanation.

322  
323  
324

17

18

19

20

21

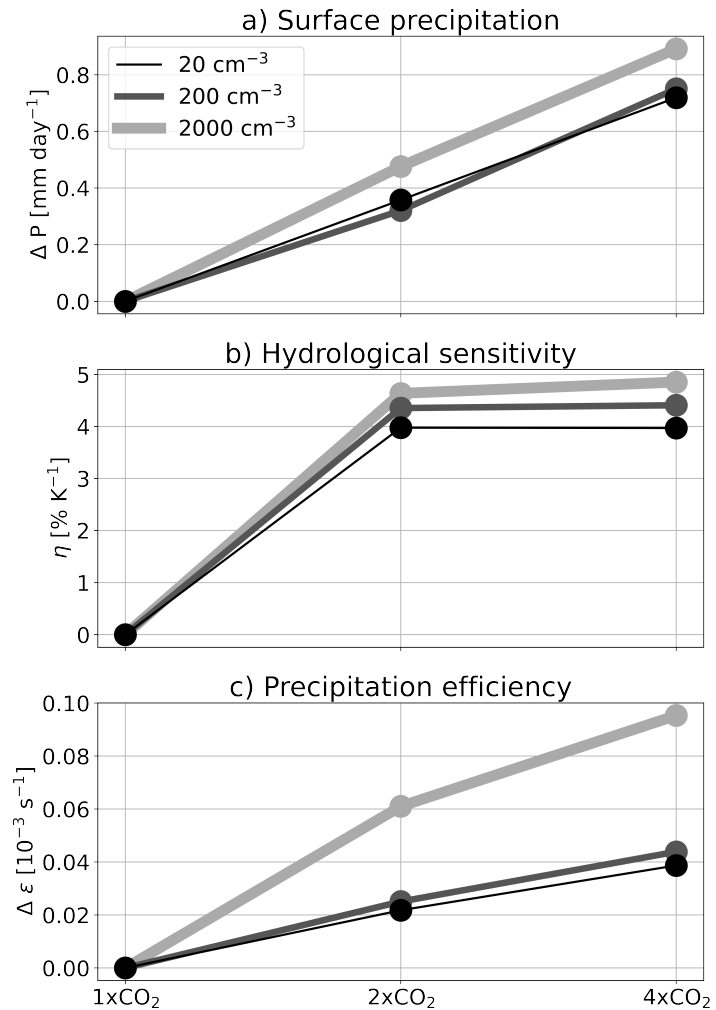
22

23

24

pnas: es

pnas: more efficiently



327

328 **Figure 5. The change in: a) surface precipitation, b) hydrological sensitivity ( $\eta$ ), and c)**  
 329 **precipitation efficiency ( $\epsilon$ ) due to a change in the CO<sub>2</sub> concentration (compared to the**  
 330 **1xCO<sub>2</sub> case of each aerosol concentration), for the different aerosol concentrations (the**  
 331 **different curves).**

332

333 The last open question is why  $\epsilon$  increases faster with CO<sub>2</sub> concentration under the  
 334 highest N<sub>a</sub> conditions. The increase in  $\epsilon$  with warming was shown to be mostly driven  
 335 by an increase in the efficiency with which cloud condensate is converted into

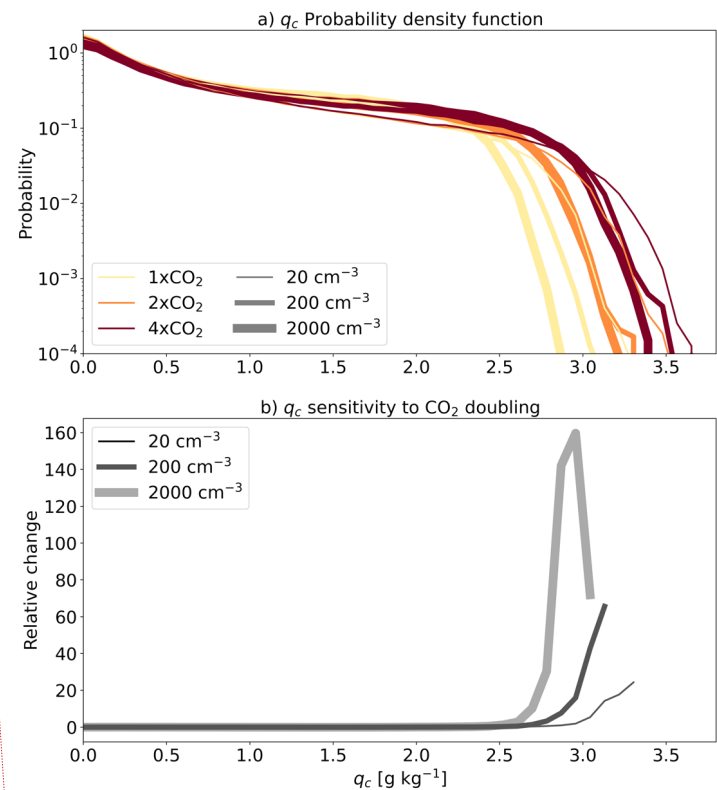
336 precipitation (Lutsko and Cronin, 2018). As was mentioned in the introduction, the  
337 conversion of cloud condensate into precipitation (or autoconversion of cloud droplets)  
338 becomes significant only when liquid water amount and/or droplet radii reach a critical  
339 threshold (Freud and Rosenfeld, 2012). To understand the faster  $\epsilon$  increases with CO<sub>2</sub>  
340 concentration under the highest  $N_a$  conditions, we present the histograms over the  
341 domain and time (during the last 150 days of the simulations based on 3D output in 1-  
342 hour resolution) of liquid cloud droplets mixing ratio ( $q_c$  – Fig. 6) and mean cloud  
343 droplet radii ( $r_c$  – Fig. 7) around the height of the maximum in cloud droplet effective  
344 radii (1950m) and its mean sensitivity to doubling of CO<sub>2</sub> concentration for each  $N_a$   
345 condition.

346 Figure 6 demonstrates that the cut-off of the  $q_c$  distribution (the mixing ratio for which  
347 the probability density function starts to decrease sharply) increases with the CO<sub>2</sub>  
348 concentration and decreases with the aerosol concentration. However, the sensitivity of  
349 the relatively large  $q_c$  with CO<sub>2</sub> concentration is significantly larger under high aerosol  
350 concentrations compared to the lower aerosol concentrations (Fig. 6b). The larger  
351 relative increase in high  $q_c$  promotes the autoconversion process and hence enhances  $\epsilon$ ,  
352 more under high aerosol concentrations than under low aerosol concentrations.

353 Figure 7 demonstrates, in line with expectations, that  $N_a$  has a strong effect on  $r_c$ . In  
354 addition, it shows that under all  $N_a$  conditions,  $r_c$  increases with the CO<sub>2</sub> concentration.  
355 This could be explained by the increase in the availability of water vapor (Fig. 2),  
356 which, for a given  $N_a$  conditions, enable larger diffusional growth of the droplets. [This  
357 trend could also be understood from the increase in  \$q\_c\$  with warming \(Fig. 6, Lutsko  
358 and Cronin 2018\), which under a given  \$N\_a\$  conditions implies larger  \$r\_c\$ .](#) Here again, the  
359 highest  $N_a$  conditions demonstrate the largest sensitivity of  $r_c$  to CO<sub>2</sub> concentration,  
360 especially at the right-hand side of the distribution (Fig. 7b). This could be explained  
361 by the fact that under these high  $N_a$  conditions, the cloud droplet growth is primarily  
362 limited by the availability of water vapor, as large number of droplets compete for the  
363 available water vapor (Koren et al., 2014; Dagan et al., 2015a; Reutter et al., 2009).

64 [Thus, an increase in the availability of water vapor with CO<sub>2</sub> concentration \(Fig. 2\)  
365 under polluted conditions results in a larger increase in  \$r\_c\$  compared with clean  
366 conditions. However, the reasons behind this trend, as well as behind the larger increase  
367 in  \$q\_c\$  in high- \$N\_a\$  simulations deserve further exploration in the future.](#) Similarly to the  
368  $q_c$  case, the larger relative increase in the relatively large droplets promotes the

369 autoconversion process and hence enhances  $\epsilon$ , more under high aerosol concentrations  
 370 than under lower aerosol concentrations.



369  
 370  
 371  
 372  
 373  
 374  
 375  
 376  
 377  
 378  
 379  
 380  
 381  
 382  
 383  
 384  
 385  
 386  
 387  
 388  
 389  
 390  
 391  
 392  
 393  
 394  
 395  
 396  
 397  
 398  
 399  
 400  
 401  
 402  
 403  
 404  
 405  
 406  
 407  
 408  
 409  
 410  
 411  
 412  
 413  
 414  
 415  
 416  
 417  
 418  
 419  
 420  
 421  
 422  
 423  
 424  
 425  
 426  
 427  
 428  
 429  
 430  
 431  
 432  
 433  
 434  
 435  
 436  
 437  
 438  
 439  
 440  
 441  
 442  
 443  
 444  
 445  
 446  
 447  
 448  
 449  
 450  
 451  
 452  
 453  
 454  
 455  
 456  
 457  
 458  
 459  
 460  
 461  
 462  
 463  
 464  
 465  
 466  
 467  
 468  
 469  
 470  
 471  
 472  
 473  
 474  
 475  
 476  
 477  
 478  
 479  
 480  
 481  
 482  
 483  
 484  
 485  
 486  
 487  
 488  
 489  
 490  
 491  
 492  
 493  
 494  
 495  
 496  
 497  
 498  
 499  
 500  
 501  
 502  
 503  
 504  
 505  
 506  
 507  
 508  
 509  
 510  
 511  
 512  
 513  
 514  
 515  
 516  
 517  
 518  
 519  
 520  
 521  
 522  
 523  
 524  
 525  
 526  
 527  
 528  
 529  
 530  
 531  
 532  
 533  
 534  
 535  
 536  
 537  
 538  
 539  
 540  
 541  
 542  
 543  
 544  
 545  
 546  
 547  
 548  
 549  
 550  
 551  
 552  
 553  
 554  
 555  
 556  
 557  
 558  
 559  
 560  
 561  
 562  
 563  
 564  
 565  
 566  
 567  
 568  
 569  
 570  
 571  
 572  
 573  
 574  
 575  
 576  
 577  
 578  
 579  
 580  
 581  
 582  
 583  
 584  
 585  
 586  
 587  
 588  
 589  
 590  
 591  
 592  
 593  
 594  
 595  
 596  
 597  
 598  
 599  
 600  
 601  
 602  
 603  
 604  
 605  
 606  
 607  
 608  
 609  
 610  
 611  
 612  
 613  
 614  
 615  
 616  
 617  
 618  
 619  
 620  
 621  
 622  
 623  
 624  
 625  
 626  
 627  
 628  
 629  
 630  
 631  
 632  
 633  
 634  
 635  
 636  
 637  
 638  
 639  
 640  
 641  
 642  
 643  
 644  
 645  
 646  
 647  
 648  
 649  
 650  
 651  
 652  
 653  
 654  
 655  
 656  
 657  
 658  
 659  
 660  
 661  
 662  
 663  
 664  
 665  
 666  
 667  
 668  
 669  
 670  
 671  
 672  
 673  
 674  
 675  
 676  
 677  
 678  
 679  
 680  
 681  
 682  
 683  
 684  
 685  
 686  
 687  
 688  
 689  
 690  
 691  
 692  
 693  
 694  
 695  
 696  
 697  
 698  
 699  
 700  
 701  
 702  
 703  
 704  
 705  
 706  
 707  
 708  
 709  
 710  
 711  
 712  
 713  
 714  
 715  
 716  
 717  
 718  
 719  
 720  
 721  
 722  
 723  
 724  
 725  
 726  
 727  
 728  
 729  
 730  
 731  
 732  
 733  
 734  
 735  
 736  
 737  
 738  
 739  
 740  
 741  
 742  
 743  
 744  
 745  
 746  
 747  
 748  
 749  
 750  
 751  
 752  
 753  
 754  
 755  
 756  
 757  
 758  
 759  
 760  
 761  
 762  
 763  
 764  
 765  
 766  
 767  
 768  
 769  
 770  
 771  
 772  
 773  
 774  
 775  
 776  
 777  
 778  
 779  
 780  
 781  
 782  
 783  
 784  
 785  
 786  
 787  
 788  
 789  
 790  
 791  
 792  
 793  
 794  
 795  
 796  
 797  
 798  
 799  
 800  
 801  
 802  
 803  
 804  
 805  
 806  
 807  
 808  
 809  
 810  
 811  
 812  
 813  
 814  
 815  
 816  
 817  
 818  
 819  
 820  
 821  
 822  
 823  
 824  
 825  
 826  
 827  
 828  
 829  
 830  
 831  
 832  
 833  
 834  
 835  
 836  
 837  
 838  
 839  
 840  
 841  
 842  
 843  
 844  
 845  
 846  
 847  
 848  
 849  
 850  
 851  
 852  
 853  
 854  
 855  
 856  
 857  
 858  
 859  
 860  
 861  
 862  
 863  
 864  
 865  
 866  
 867  
 868  
 869  
 870  
 871  
 872  
 873  
 874  
 875  
 876  
 877  
 878  
 879  
 880  
 881  
 882  
 883  
 884  
 885  
 886  
 887  
 888  
 889  
 890  
 891  
 892  
 893  
 894  
 895  
 896  
 897  
 898  
 899  
 900  
 901  
 902  
 903  
 904  
 905  
 906  
 907  
 908  
 909  
 910  
 911  
 912  
 913  
 914  
 915  
 916  
 917  
 918  
 919  
 920  
 921  
 922  
 923  
 924  
 925  
 926  
 927  
 928  
 929  
 930  
 931  
 932  
 933  
 934  
 935  
 936  
 937  
 938  
 939  
 940  
 941  
 942  
 943  
 944  
 945  
 946  
 947  
 948  
 949  
 950  
 951  
 952  
 953  
 954  
 955  
 956  
 957  
 958  
 959  
 960  
 961  
 962  
 963  
 964  
 965  
 966  
 967  
 968  
 969  
 970  
 971  
 972  
 973  
 974  
 975  
 976  
 977  
 978  
 979  
 980  
 981  
 982  
 983  
 984  
 985  
 986  
 987  
 988  
 989  
 990  
 991  
 992  
 993  
 994  
 995  
 996  
 997  
 998  
 999  
 1000  
 1001  
 1002  
 1003  
 1004  
 1005  
 1006  
 1007  
 1008  
 1009  
 1010  
 1011  
 1012  
 1013  
 1014  
 1015  
 1016  
 1017  
 1018  
 1019  
 1020  
 1021  
 1022  
 1023  
 1024  
 1025  
 1026  
 1027  
 1028  
 1029  
 1030  
 1031  
 1032  
 1033  
 1034  
 1035  
 1036  
 1037  
 1038  
 1039  
 1040  
 1041  
 1042  
 1043  
 1044  
 1045  
 1046  
 1047  
 1048  
 1049  
 1050  
 1051  
 1052  
 1053  
 1054  
 1055  
 1056  
 1057  
 1058  
 1059  
 1060  
 1061  
 1062  
 1063  
 1064  
 1065  
 1066  
 1067  
 1068  
 1069  
 1070  
 1071  
 1072  
 1073  
 1074  
 1075  
 1076  
 1077  
 1078  
 1079  
 1080  
 1081  
 1082  
 1083  
 1084  
 1085  
 1086  
 1087  
 1088  
 1089  
 1090  
 1091  
 1092  
 1093  
 1094  
 1095  
 1096  
 1097  
 1098  
 1099  
 1100  
 1101  
 1102  
 1103  
 1104  
 1105  
 1106  
 1107  
 1108  
 1109  
 1110  
 1111  
 1112  
 1113  
 1114  
 1115  
 1116  
 1117  
 1118  
 1119  
 1120  
 1121  
 1122  
 1123  
 1124  
 1125  
 1126  
 1127  
 1128  
 1129  
 1130  
 1131  
 1132  
 1133  
 1134  
 1135  
 1136  
 1137  
 1138  
 1139  
 1140  
 1141  
 1142  
 1143  
 1144  
 1145  
 1146  
 1147  
 1148  
 1149  
 1150  
 1151  
 1152  
 1153  
 1154  
 1155  
 1156  
 1157  
 1158  
 1159  
 1160  
 1161  
 1162  
 1163  
 1164  
 1165  
 1166  
 1167  
 1168  
 1169  
 1170  
 1171  
 1172  
 1173  
 1174  
 1175  
 1176  
 1177  
 1178  
 1179  
 1180  
 1181  
 1182  
 1183  
 1184  
 1185  
 1186  
 1187  
 1188  
 1189  
 1190  
 1191  
 1192  
 1193  
 1194  
 1195  
 1196  
 1197  
 1198  
 1199  
 1200  
 1201  
 1202  
 1203  
 1204  
 1205  
 1206  
 1207  
 1208  
 1209  
 1210  
 1211  
 1212  
 1213  
 1214  
 1215  
 1216  
 1217  
 1218  
 1219  
 1220  
 1221  
 1222  
 1223  
 1224  
 1225  
 1226  
 1227  
 1228  
 1229  
 1230  
 1231  
 1232  
 1233  
 1234  
 1235  
 1236  
 1237  
 1238  
 1239  
 1240  
 1241  
 1242  
 1243  
 1244  
 1245  
 1246  
 1247  
 1248  
 1249  
 1250  
 1251  
 1252  
 1253  
 1254  
 1255  
 1256  
 1257  
 1258  
 1259  
 1260  
 1261  
 1262  
 1263  
 1264  
 1265  
 1266  
 1267  
 1268  
 1269  
 1270  
 1271  
 1272  
 1273  
 1274  
 1275  
 1276  
 1277  
 1278  
 1279  
 1280  
 1281  
 1282  
 1283  
 1284  
 1285  
 1286  
 1287  
 1288  
 1289  
 1290  
 1291  
 1292  
 1293  
 1294  
 1295  
 1296  
 1297  
 1298  
 1299  
 1300  
 1301  
 1302  
 1303  
 1304  
 1305  
 1306  
 1307  
 1308  
 1309  
 1310  
 1311  
 1312  
 1313  
 1314  
 1315  
 1316  
 1317  
 1318  
 1319  
 1320  
 1321  
 1322  
 1323  
 1324  
 1325  
 1326  
 1327  
 1328  
 1329  
 1330  
 1331  
 1332  
 1333  
 1334  
 1335  
 1336  
 1337  
 1338  
 1339  
 1340  
 1341  
 1342  
 1343  
 1344  
 1345  
 1346  
 1347  
 1348  
 1349  
 1350  
 1351  
 1352  
 1353  
 1354  
 1355  
 1356  
 1357  
 1358  
 1359  
 1360  
 1361  
 1362  
 1363  
 1364  
 1365  
 1366  
 1367  
 1368  
 1369  
 1370  
 1371  
 1372  
 1373  
 1374  
 1375  
 1376  
 1377  
 1378  
 1379  
 1380  
 1381  
 1382  
 1383  
 1384  
 1385  
 1386  
 1387  
 1388  
 1389  
 1390  
 1391  
 1392  
 1393  
 1394  
 1395  
 1396  
 1397  
 1398  
 1399  
 1400  
 1401  
 1402  
 1403  
 1404  
 1405  
 1406  
 1407  
 1408  
 1409  
 1410  
 1411  
 1412  
 1413  
 1414  
 1415  
 1416  
 1417  
 1418  
 1419  
 1420  
 1421  
 1422  
 1423  
 1424  
 1425  
 1426  
 1427  
 1428  
 1429  
 1430  
 1431  
 1432  
 1433  
 1434  
 1435  
 1436  
 1437  
 1438  
 1439  
 1440  
 1441  
 1442  
 1443  
 1444  
 1445  
 1446  
 1447  
 1448  
 1449  
 1450  
 1451  
 1452  
 1453  
 1454  
 1455  
 1456  
 1457  
 1458  
 1459  
 1460  
 1461  
 1462  
 1463  
 1464  
 1465  
 1466  
 1467  
 1468  
 1469  
 1470  
 1471  
 1472  
 1473  
 1474  
 1475  
 1476  
 1477  
 1478  
 1479  
 1480  
 1481  
 1482  
 1483  
 1484  
 1485  
 1486  
 1487  
 1488  
 1489  
 1490  
 1491  
 1492  
 1493  
 1494  
 1495  
 1496  
 1497  
 1498  
 1499  
 1500  
 1501  
 1502  
 1503  
 1504  
 1505  
 1506  
 1507  
 1508  
 1509  
 1510  
 1511  
 1512  
 1513  
 1514  
 1515  
 1516  
 1517  
 1518  
 1519  
 1520  
 1521  
 1522  
 1523  
 1524  
 1525  
 1526  
 1527  
 1528  
 1529  
 1530  
 1531  
 1532  
 1533  
 1534  
 1535  
 1536  
 1537  
 1538  
 1539  
 1540  
 1541  
 1542  
 1543  
 1544  
 1545  
 1546  
 1547  
 1548  
 1549  
 1550  
 1551  
 1552  
 1553  
 1554  
 1555  
 1556  
 1557  
 1558  
 1559  
 1560  
 1561  
 1562  
 1563  
 1564  
 1565  
 1566  
 1567  
 1568  
 1569  
 1570  
 1571  
 1572  
 1573  
 1574  
 1575  
 1576  
 1577  
 1578  
 1579  
 1580  
 1581  
 1582  
 1583  
 1584  
 1585  
 1586  
 1587  
 1588  
 1589  
 1590  
 1591  
 1592  
 1593  
 1594  
 1595  
 1596  
 1597  
 1598  
 1599  
 1600  
 1601  
 1602  
 1603  
 1604  
 1605  
 1606  
 1607  
 1608  
 1609  
 1610  
 1611  
 1612  
 1613  
 1614  
 1615  
 1616  
 1617  
 1618  
 1619  
 1620  
 1621  
 1622  
 1623  
 1624  
 1625  
 1626  
 1627  
 1628  
 1629  
 1630  
 1631  
 1632  
 1633  
 1634  
 1635  
 1636  
 1637  
 1638  
 1639  
 1640  
 1641  
 1642  
 1643  
 1644  
 1645  
 1646  
 1647  
 1648  
 1649  
 1650  
 1651  
 1652  
 1653  
 1654  
 1655  
 1656  
 1657  
 1658  
 1659  
 1660  
 1661  
 1662  
 1663  
 1664  
 1665  
 1666  
 1667  
 1668  
 1669  
 1670  
 1671  
 1672  
 1673  
 1674  
 1675  
 1676  
 1677  
 1678  
 1679  
 1680  
 1681  
 1682  
 1683  
 1684  
 1685  
 1686  
 1687  
 1688  
 1689  
 1690  
 1691  
 1692  
 1693  
 1694  
 1695  
 1696  
 1697  
 1698  
 1699  
 1700  
 1701  
 1702  
 1703  
 1704  
 1705  
 1706  
 1707  
 1708  
 1709  
 1710  
 1711  
 1712  
 1713  
 1714  
 1715  
 1716  
 1717  
 1718  
 1719  
 1720  
 1721  
 1722  
 1723  
 1724  
 1725  
 1726  
 1727  
 1728  
 1729  
 1730  
 1731  
 1732  
 1733  
 1734  
 1735  
 1736  
 1737  
 1738  
 1739  
 1740  
 1741  
 1742  
 1743  
 1744  
 1745  
 1746  
 1747  
 1748  
 1749  
 1750  
 1751  
 1752  
 1753  
 1754  
 1755  
 1756  
 1757  
 1758  
 1759  
 1760  
 1761  
 1762  
 1763  
 1764

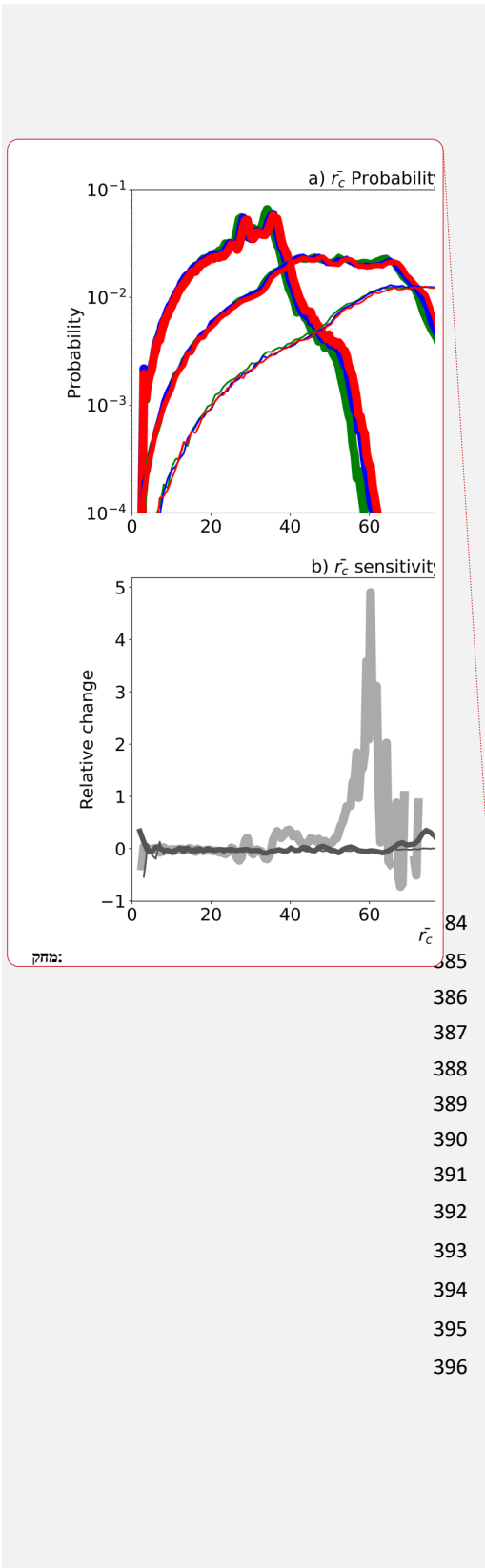


Figure 7. Probability density functions (PDF) of cloud droplet mean radii ( $r_c$ ) for the different simulations (a), and the mean sensitivity of the  $r_c$  PDF to a doubling of the CO<sub>2</sub> concentration based on the three combinations available for each  $N_a$  condition [2xCO<sub>2</sub>-1xCO<sub>2</sub>, 4xCO<sub>2</sub>-2xCO<sub>2</sub> and (4xCO<sub>2</sub>-1xCO<sub>2</sub>)/2] (b), calculated for the heights around which the cloud droplet effective radii reach a maximum (1950m) and using 3-D files output every hour of the last 150 days of the simulations. Note the logarithmic scales for the y-axes of a.

#### 4. Summary and conclusions

The role of clouds in a climate-change is manifested by two pathways: (1) effects of anthropogenic aerosol on clouds, and (2) feedback that clouds exert on the changing climate. These two pathways are usually studied separately, and even by different

398 scientific communities. In this paper, we demonstrate that the two pathways are closely  
399 linked to each other and should be examined concurrently.

400 Using long, idealized RCE simulations over a small domain with a slab ocean model,  
401 we demonstrate that the ECS, i.e., the increase in surface temperature under equilibrium  
402 conditions due to doubling of the CO<sub>2</sub> concentration, increases with the aerosol  
403 concentration. The ECS increase is explained by a faster increase in precipitation  
404 efficiency with warming under high aerosol concentrations, which [represents a more](#)  
405 [efficient depletion of](#) the water from the cloud and thus is manifested as an increase in  
406 the cloud feedback parameter. The precipitation efficiency increases faster under high  
407 aerosol concentration due to a higher sensitivity of the relatively high liquid water  
408 mixing ratios and the relatively large mean droplet sizes to a CO<sub>2</sub> concentration  
409 increase. [We note that the increase in the total \(shortwave plus longwave\) cloud](#)  
410 [feedback parameter with the increase in precipitation efficiency is a result of a stronger](#)  
411 [shortwave effect \(Li et al., 2019\) than a longwave effect \(Lindzen et al., 2001\) in the](#)  
412 [simulations presented here. Future work should examine the robustness of this trend in](#)  
413 [different models, and with different microphysical and radiative schemes. Moreover,](#)  
414 [the response of precipitation to changes in aerosol concentration might be](#)  
415 [microphysical representation depended](#) (White et al., 2017), [and hence should be](#)  
416 [examined in the future under different microphysical schemes \(conceivably in a multi-](#)  
417 [model intercomparison project focusing on aerosol effect on RCE simulations\).](#)

418 The results presented here are based on idealized simulations over a small domain.  
419 Under more realistic conditions, other processes, not included here, that could affect  
420 the precipitation efficiency and hence the general trend will be introduced. In particular,  
421 convective self-aggregation could be of interest as, while it is inhibited in the small  
422 domain used here, it was shown to affect precipitation efficiency (Lutsko et al., 2021)  
423 and to be affected by aerosols (Nishant et al., 2019). Other processes that should be  
424 accounted for in future research include the presence of large-scale circulation and  
425 direct aerosol radiative effects (Dagan et al., 2019; Dingley et al., 2021). [In addition,](#)  
426 [the results presented here suggest that the sensitivity of ECS to aerosol loading might](#)  
427 [not be linear \(Table 1\). Hence, the dynamical aerosol range present at different](#)  
428 [geographical locations would affect the total ECS trend.](#)

429 The results presented here suggest a [possible](#) connection between cloud feedback and  
430 aerosol-cloud interactions. The regulation of aerosol emissions is known to be more  
431 effective than the effort to reduce greenhouse gas emissions. This, together with the

436 short lifetime of aerosols in the atmosphere, has resulted in a reduction in the value of  
437 the global mean aerosol effective radiative forcing in recent years (Quaas et al., 2022).  
438 If the conclusions of this paper hold under higher levels of complexity (e.g., large-scale  
439 circulation, convective self-aggregation, etc.) this might mean that the reduction in  
440 global aerosol emissions could lead to a reduction in ECS, which could compensate, at  
441 least partially, for the reduction in the negative forcing induced by aerosols (Quaas et  
442 al., 2022; Bellouin et al., 2019), thus providing yet additional motivation for reducing  
443 aerosol emissions globally.

445 Code availability

446 SAM is publicly available at: <http://rossby.msrc.sunysb.edu/~marat/SAM.html>

448 Data availability

49 The data presented in this study is publicly available at:  
50 <https://doi.org/10.5281/zenodo.7306706>

## 452 Author contributions

453 GD carried out the simulations and analyses presented and prepared the article.

455 Competing interests

456 The authors declare that they have no conflict of interest.

458 Financial support

459 This research was supported by the Israeli Science Foundation Grant (1419/21).

## 5. References

Abbott, T. H., & Cronin, T. W. (2021). Aerosol invigoration of atmospheric convection through increases in humidity. *science*, 371(6524), 83-85.

Albrecht, B. A.: Aerosols, cloud microphysics, and fractional cloudiness, *Science* (New York, NY), 245, 1227, 1989.

Bellouin, N., Quaas, J., Gryspenert, E., Kinne, S., Stier, P., Watson-Parris, D., Boucher, O., Carslaw, K., Christensen, M., and Daniau, A.-L.: Bounding aerosol radiative forcing of climate change, *Reviews of Geophysics*, 2019.

Ceppi, P., Brient, F., Zelinka, M. D., and Hartmann, D. L.: Cloud feedback mechanisms and their representation in global climate models, *WIREs Climate Change*, 2017.

Collins, W. D., Rasch, P. J., Boville, B. A., Hack, J. J., McCaa, J. R., Williamson, D. L., Briegleb, B. P., Bitz, C. M., Lin, S.-J., and Zhang, M.: The formulation and

475 atmospheric simulation of the Community Atmosphere Model version 3 (CAM3),  
 476 Journal of Climate, 19, 2144-2161, 2006.

477 Dagan, G., Koren, I., and Altaratz, O.: Competition between core and periphery-based  
 478 processes in warm convective clouds—from invigoration to suppression, Atmospheric  
 479 Chemistry and Physics, 15, 2749-2760, 2015a.

480 Dagan, G., Koren, I., and Altaratz, O.: Aerosol effects on the timing of warm rain  
 481 processes, Geophysical Research Letters, 42, 4590-4598, 10.1002/2015GL063839,  
 482 2015b.

483 Dagan, G., Stier, P., and Watson-Parris, D.: Contrasting response of precipitation to  
 484 aerosol perturbation in the tropics and extra-tropics explained by energy budget  
 485 considerations, Geophysical Research Letters, 2019.

486 Dingley, B., Dagan, G., and Stier, P.: Forcing convection to aggregate using diabatic  
 487 heating perturbations, Journal of Advances in Modeling Earth Systems, 13,  
 488 e2021MS002579, 2021.

489 Freud, E., and Rosenfeld, D.: Linear relation between convective cloud drop number  
 490 concentration and depth for rain initiation, Journal of Geophysical Research:  
 491 Atmospheres (1984–2012), 117, 2012.

492 Gettelman, A., and Sherwood, S.: Processes Responsible for Cloud Feedback, Current  
 493 Climate Change Reports, 2, 179-189, 2016.

494 Held, I. M., and Soden, B. J.: Robust responses of the hydrological cycle to global  
 495 warming, Journal of Climate, 19, 5686-5699, 2006.

496 Igel, A. L., and van den Heever, S. C.: Invigoration or Enervation of Convective Clouds  
 497 by Aerosols?, Geophysical Research Letters, 48, e2021GL093804, 2021.

498 Khain, A. P.: Notes on state-of-the-art investigations of aerosol effects on precipitation:  
 499 a critical review, Environmental Research Letters, 4, 015004 (015020 pp.)-015004  
 500 (015020 pp.), 10.1088/1748-9326/4/1/015004, 2009.

501 Khairoutdinov, M., and Yang, C.-E.: Cloud-resolving modelling of aerosol indirect  
 502 effects in idealised radiative-convective equilibrium with interactive and fixed sea  
 503 surface temperature, Atmospheric Chemistry and Physics, 13, 4133-4144, 2013.

504 Khairoutdinov, M. F., and Randall, D. A.: Cloud resolving modeling of the ARM  
 505 summer 1997 IOP: Model formulation, results, uncertainties, and sensitivities, Journal  
 506 of the Atmospheric Sciences, 60, 2003.

507 [Koren, I., Kaufman, Y. J., Rosenfeld, D., Remer, L. A., & Rudich, Y. \(2005\). Aerosol](#)  
 508 [invigoration and restructuring of Atlantic convective clouds. \*Geophysical research\*](#)  
 509 [letters, 32\(14\). \(](#)

510 [Koren, I., Altaratz, O., Remer, L. A., Feingold, G., Martins, J. V., & Heiblum, R. H.](#)  
 511 [\(2012\). Aerosol-induced intensification of rain from the tropics to the mid-latitudes.](#)  
 512 [Nature Geoscience.](#)

513 Koren, I., Dagan, G., and Altaratz, O.: From aerosol-limited to invigoration of warm  
 514 convective clouds, science, 344, 1143-1146, 2014.

515 Li, R., Storelvmo, T., Fedorov, A. V., and Choi, Y.-S.: A positive IRIS feedback:  
 516 Insights from climate simulations with temperature-sensitive cloud-rain conversion,  
 517 Journal of climate, 32, 5305-5324, 2019.

518 Li, R. L., Studholme, J. H., Fedorov, A. V., and Storelvmo, T.: Precipitation efficiency  
 519 constraint on climate change, Nature Climate Change, 12, 642-648, 2022.

520 Lindzen, R. S., Chou, M.-D., and Hou, A. Y.: Does the earth have an adaptive infrared  
 521 iris?, Bulletin of the American Meteorological Society, 82, 417-432, 2001.

522 Loeb, N. G., Doelling, D. R., Wang, H., Su, W., Nguyen, C., Corbett, J. G., Liang, L.,  
 523 Mitrescu, C., Rose, F. G., and Kato, S.: Clouds and the earth’s radiant energy system

524 (CERES) energy balanced and filled (EBAF) top-of-atmosphere (TOA) edition-4.0  
525 data product, *Journal of Climate*, 31, 895-918, 2018.

526 Lutsko, N., Sherwood, S. C., and Zhao, M.: Precipitation Efficiency and Climate  
527 Sensitivity (Invited Chapter for the AGU Geophysical Monograph Series" Clouds and  
528 Climate"), 2021.

529 Lutsko, N. J., and Cronin, T. W.: Increase in precipitation efficiency with surface  
530 warming in radiative-convective equilibrium, *Journal of Advances in Modeling Earth  
531 Systems*, 10, 2992-3010, 2018.

532 Mauritsen, T., and Stevens, B.: Missing iris effect as a possible cause of muted  
533 hydrological change and high climate sensitivity in models, *Nature Geoscience*, 8, 346,  
534 2015.

535 Morrison, H., Curry, J., and Khvorostyanov, V.: A new double-moment microphysics  
536 parameterization for application in cloud and climate models. Part I: Description,  
537 *Journal of the atmospheric sciences*, 62, 1665-1677, 2005.

538 Muller, C. J., and Held, I. M.: Detailed investigation of the self-aggregation of  
539 convection in cloud-resolving simulations, *Journal of the Atmospheric Sciences*, 69,  
540 2551-2565, 2012.

541 Mülmenstädt, J., and Feingold, G.: The Radiative Forcing of Aerosol-Cloud  
542 Interactions in Liquid Clouds: Wrestling and Embracing Uncertainty, *Current Climate  
543 Change Reports*, 4, 23-40, 2018.

544 Nishant, N., Sherwood, S. C., and Geoffroy, O.: Aerosol-induced modification of  
545 organised convection and top-of-atmosphere radiation, *npj Climate and Atmospheric  
546 Science*, 2, 1-10, 2019.

547 Nuijens, L., and Siebesma, A. P.: Boundary Layer Clouds and Convection over  
548 Subtropical Oceans in our Current and in a Warmer Climate, *Current Climate Change  
549 Reports*, 1-15, 2019.

550 Quaas, J., Jia, H., Smith, C., Albright, A. L., Aas, W., Bellouin, N., Boucher, O.,  
551 Doutriaux-Boucher, M., Forster, P. M., and Grosvenor, D.: Robust evidence for  
552 reversal in the aerosol effective climate forcing trend, *Atmospheric Chemistry and  
553 Physics Discussions*, 1-25, 2022.

554 Reutter, P., Su, H., Trentmann, J., Simmel, M., Rose, D., Gunthe, S., Wernli, H.,  
555 Andreae, M., and Pöschl, U.: Aerosol-and updraft-limited regimes of cloud droplet  
556 formation: influence of particle number, size and hygroscopicity on the activation of  
557 cloud condensation nuclei (CCN), *Atmospheric Chemistry and Physics*, 9, 7067-7080,  
558 2009.

559 Romps, D. M.: Climate sensitivity and the direct effect of carbon dioxide in a limited-  
560 area cloud-resolving model, *Journal of Climate*, 33, 3413-3429, 2020.

561 Rosenfeld, D.: Suppression of rain and snow by urban and industrial air pollution,  
562 *Science*, 287, 1793-1796, 10.1126/science.287.5459.1793, 2000.

563 [Rosenfeld, D., Lohmann, U., Raga, G. B., O'Dowd, C. D., Kulmala, M., Fuzzi, S., et al. \(2008\). Flood or drought: How do aerosols affect precipitation? science, 321\(5894\), 1309-1313. <Go to ISI>://WOS:000258914300038](#)

564 Schneider, T., Teixeira, J., Bretherton, C. S., Brient, F., Pressel, K. G., Schär, C., and  
565 Siebesma, A. P.: Climate goals and computing the future of clouds, *Nature Climate  
566 Change*, 7, 3-5, 2017.

567 Sherwood, S., Webb, M. J., Annan, J. D., Armour, K., Forster, P. M., Hargreaves, J. C.,  
568 Hegerl, G., Klein, S. A., Marvel, K. D., and Rohling, E. J.: An assessment of Earth's  
569 climate sensitivity using multiple lines of evidence, *Reviews of Geophysics*, 58,  
570 e2019RG000678, 2020.

571

572

573 Twomey, S.: The nuclei of natural cloud formation part II: The supersaturation in  
574 natural clouds and the variation of cloud droplet concentration, *Geofisica pura e*  
575 *applicata*, 43, 243-249, 1959.

576 Twomey, S.: Pollution and the planetary albedo, *Atmospheric Environment* (1967), 8,  
577 1251-1256, 1974.

578 Twomey, S.: The influence of pollution on the shortwave albedo of clouds, *Journal of*  
579 *the atmospheric sciences*, 34, 1149-1152, 1977.

580 Warner, J., and Twomey, S.: The production of cloud nuclei by cane fires and the effect

581 on cloud droplet concentration, *Journal of the atmospheric Sciences*, 24, 704-706, 1967.

מעובב: מושナル לימוי

582 82 → White, B., Gryspeerdt, E., Stier, P., Morrison, H., Thompson, G., & Kipling, Z. (2017).  
583 Uncertainty from choice of microphysics scheme in convection-permitting models  
584 significantly exceeds aerosol effects. *Atmospheric Chemistry and Physics*, 7.

585 Wing, A. A., Reed, K. A., Satoh, M., Stevens, B., Bony, S., and Ohno, T.: Radiative-  
586 convective equilibrium model intercomparison project, *Geoscientific Model*  
587 *Development*, 793-813, 2018.

588 Yanase, T., Nishizawa, S., Miura, H., Takemi, T., and Tomita, H.: New critical length  
589 for the onset of self-aggregation of moist convection, *Geophysical Research Letters*,  
590 47, e2020GL088763, 2020.

591

592

מעובב: מושナル לימוי

93 →

94

רשות: Koren, I., Altaratz, O., Remer, L. A., Feingold, G.,  
Martins, J. V., & Heiblum, R. H. (2012). Aerosol-induced  
intensification of rain from the tropics to the mid-

latitudes. *Nature Geoscience*.

Koren, I., Kaufman, Y. J., Rosenfeld, D., Remer, L. A., &  
Rudich, Y. (2005). Aerosol invigoration and restructuring of  
Atlantic convective clouds. *Geophysical research letters*,  
32(14).

Rosenfeld, D., Lohmann, U., Raga, G. B., O'Dowd, C. D.,  
Kulmala, M., Fuzzi, S., et al. (2008). Flood or drought: How  
do aerosols affect precipitation? *science*, 321(5894), 1309-  
1313. <Go to ISI>://WOS:000258914300038

White, B., Gryspeerdt, E., Stier, P., Morrison, H.,  
Thompson, G., & Kipling, Z. (2017). Uncertainty from  
choice of microphysics scheme in convection-permitting  
models significantly exceeds aerosol effects. *Atmospheric  
Chemistry and Physics*, 7.